International Journal of Technology

http://ijtech.eng.ui.ac.id

Research Article

Multi-Objective Optimization of a Neuro-Fuzzy Controller Using Non-dominated Sorting Genetic Algorithm II for Robust Stabilization of the Van de Vusse Reactor

Gustavo A. Flores Fernandez[1*], Miguel Jiménez-Carrión[2], María L. Muro Zúñiga[1], Juan M. Oliva Núñez[1], María Y. Albuquerque Trelles [1]

[1]Science Area, Universidad Tecnológica del Perú, Piura, 20001, Peru

[2]Faculty of Industrial Engineering, Universidad Nacional de Piura, Castilla-Piura, 20002, Perú

[*]Corresponding author: c31035@utp.edu.pe; Tel.: +51-980367572; Fax.: +51-980367572

Abstract: A multi-objective neuro-fuzzy control strategy is proposed for a Van de Vusse continuous stirred tank reactor (CSTR), a benchmark system characterized by nonlinear dynamics and non-minimum phase behavior. The controller is based on a multi-input multi-output adaptive neuro-fuzzy inference system (ANFIS) whose parameters are optimized using the NSGA-II algorithm. The proposed framework adjusts membership functions, rule consequents, and integral gains simultaneously within a Pareto-based formulation that considers tracking performance (ITAE) and control effort. The results of the closed-loop simulation indicate improved performance compared to a classically tuned parallel PID controller and a non-optimized ANFIS baseline. The optimized controller reduces the ITAE from 159.17 (PID) and 50.29 (baseline ANFIS) to 2.51, while operating within thermal safety constraints. The controller can compensate for the inverse response dynamics within the simulated conditions. Robustness analysis under ±10% parametric uncertainty demonstrates stable performance within the evaluated scenario, although broader uncertainties, such as measurement noise and actuator dynamics, were not considered. Targeted ANOVA provides limited insight into the influence of selected integral gains, identifying the flow-related gain as a relevant factor, but does not constitute a comprehensive statistical validation of the full controller structure. Overall, the proposed ANFIS–NSGA-II framework is presented as a simulation-based proof of concept that shows potential for nonlinear process control. However, further validation under more realistic conditions and experimental implementation is required to assess its practical applicability and generalizability.

Keywords: Neuro-fuzzy control; Nonlinear systems; Non-minimum phase systems; NSGA-II; Van de Vusse reactor

1. Introduction

In the modern chemical industry, the efficient and reliable operation of nonlinear reactors, such as the continuous stirred tank reactor (CSTR), remains essential for the production of pharmaceuticals, polymers, and fine chemicals. However, their control is challenging due to strong nonlinearities, complex reaction kinetics, and multivariate coupling (Hofer et al., 2023; Rangaiah et al., 2020; Seborg et al., 2010). The Van de Vusse reactor is a benchmark system for studying competitive and consecutive reactions (A → B → C and 2A → D), and its non-minimum phase behavior, manifested through inverse response dynamics, limits achievable control performance and compromises stability (Hofer et al., 2023).

Conventional proportional-integral-derivative (PID) control often performs poorly under nonlinear dynamics, inverse responses, and time-varying delays (Alfaro-Balaguer et al., 2025; Åström and Hägglund, 2006), while its robustness under parametric uncertainty and model mismatch is limited by its dependence on accurate mathematical models (Lamba and Raghu, 2013). Model predictive control (MPC) addresses constraints and multivariable interactions,

https://doi.org/10.14716/ijtech.v17i3.8430
Received February 2026; Revised March 2026; Accepted April 2026

but its computational burden restricts its use in fast, highly nonlinear systems (Lima et al., 2023). Sliding mode control is robust against disturbances, but chattering can damage actuator performance and long-term operation (Mousavi et al., 2024; Davila et al., 2005).

Computational intelligence techniques have therefore gained attention because of their flexibility and model-free nature. Fuzzy logic control has shown effectiveness in highly nonlinear engineering applications, such as electromagnetic transmission systems (Rahman et al., 2022). The Adaptive Neuro-Fuzzy Inference System (ANFIS) combines neural learning with fuzzy inference and offers strong approximation capabilities and improved interpretability compared with conventional black-box models (Hofer et al., 2023; Rangaiah et al., 2020; Aghbashlo et al., 2016). However, training ANFIS architectures in non-minimum phase systems remains difficult because gradient-based optimization methods are often trapped in local minima associated with unstable zeros (Bagheri and Mognjerdi, 2013). In addition, modern Industry 4.0 applications require controllers that are accurate, computationally efficient, and explainable, which exposes limitations in type-2 fuzzy systems and deep reinforcement learning approaches (Liu et al., 2025; Nabil et al., 2024; Bertone et al., 2018).

Optimization is also central to improving performance and sustainability in complex chemical processes, from electrochemical reactor design for CO_2 reduction (Widiatmoko et al., 2025) to advanced control tuning. In the Van de Vusse reactor, control design is naturally a multi-objective problem that requires balancing tracking performance, dynamic response, and operational safety. Single-objective formulations often fail to capture these competing requirements, whereas multi-objective evolutionary algorithms, especially NSGA-II, can generate diverse Pareto-optimal solutions in complex dynamic systems (Zhu et al., 2022; Reyes et al., 2009; Coello Coello, 2006; Deb et al., 2002; Verma et al., 2021; Jiang and Wang, 2025; Liu et al., 2024). However, their application to the simultaneous structural and parametric design of ANFIS controllers in non-minimum phase systems remains limited, particularly in chemical process control where nonlinearities, inverse responses, and uncertainties must be addressed together (Aguilar-López et al., 2021; Prokop et al., 2020; Sevindik et al., 2024; Mohamed et al., 2025).

In this study, a multi-objective neuro-fuzzy control strategy for the Van de Vusse reactor is proposed and optimized using the NSGA-II algorithm. The main contribution is the simultaneous evolution of the ANFIS architecture's consequent parameters and membership functions within a Pareto-based optimization framework. This co-design approach explicitly incorporates tracking error and control effort to obtain an optimal trade-off between response speed and damping under severe inverse response conditions. The optimized controller is compared with classical control strategies and single-objective optimization approaches, while robustness is evaluated under parametric perturbations relevant to process intensification (Hesami et al., 2020; Fraga, 2019). The aim is to establish a scalable, interpretable, and high-performance simulation-based proof of concept for controlling complex nonlinear chemical processes.

2. Methods

The development methodology employed in this research is described in an integrated manner, structured into four main phases. In the first phase, system modeling is performed by formulating the nonlinear differential equations that describe the mass and energy balances of the Van de Vusse reactor to capture the dynamics of the consecutive and competitive reactions that originate the nonminimum phase and the multiplicity of steady states (Marquez-Vera et al., 2012). Similarly, kinetic parameters based on the Arrhenius law and operational safety constraints, such as temperature and flow limits, are established to reproduce realistic industrial conditions and ensure the simulation's physical validity (Velioglu et al., 2024).

The tracking error and its derivative are used as input variables, represented by Gaussian membership functions due to their smoothness and differentiability, facilitating training (Dostal and Bobal, 2012; Govindharaj et al., 2024; Talpur et al., 2023). The system is completed with a first-order Takagi-Sugeno rule base, whose linear consequents reduce computational cost and favor its application in real-time adaptive control.

The third phase corresponds to the multi-objective evolutionary optimization using the NSGA-II algorithm (Jiang and Wang, 2025; Liu et al., 2024; Verma et al., 2021). To avoid premature convergence, a candidate population of solutions distributed in the search space is initially generated (Deb et al., 2002). Each individual is evaluated through dynamic simulation of the reactor, calculating performance indices that penalize both error and excessive actuator usage (Bagheri and Khodabakhshian, 2014). Two conflicting objectives are considered: minimizing the ITAE index to improve precision and reducing control effort to preserve actuators (Dostal and Bobal, 2012). Subsequently, to maintain diversity, solutions are ordered using Pareto dominance and crowding distance, applying SBX crossover and polynomial mutation genetic operators to generate new solutions and explore the search space (Deb et al., 2002). Finally, a compromise solution that adequately balances the system's speed and stability is selected (Deb et al., 2002).

In the fourth phase, the optimized controller is validated, and the results are statistically analyzed. Time series of process variables are collected despite perturbations and reference changes to evaluate system robustness (Velioglu et al., 2024). Subsequently, an analysis of variance (ANOVA) is applied to determine the statistical significance of the observed performance differences (Coello Coello, 2004), followed by Duncan's multiple range post-hoc test to identify which strategies present significantly superior performance (Odwyer, 2009). Finally, graphical representations are generated, including the Pareto frontier and comparative diagrams, to facilitate the visual interpretation of results and evidence the superiority of the proposed method (Coello, 2002). All the aforementioned steps are summarized in the following flow chart (Figure 1):

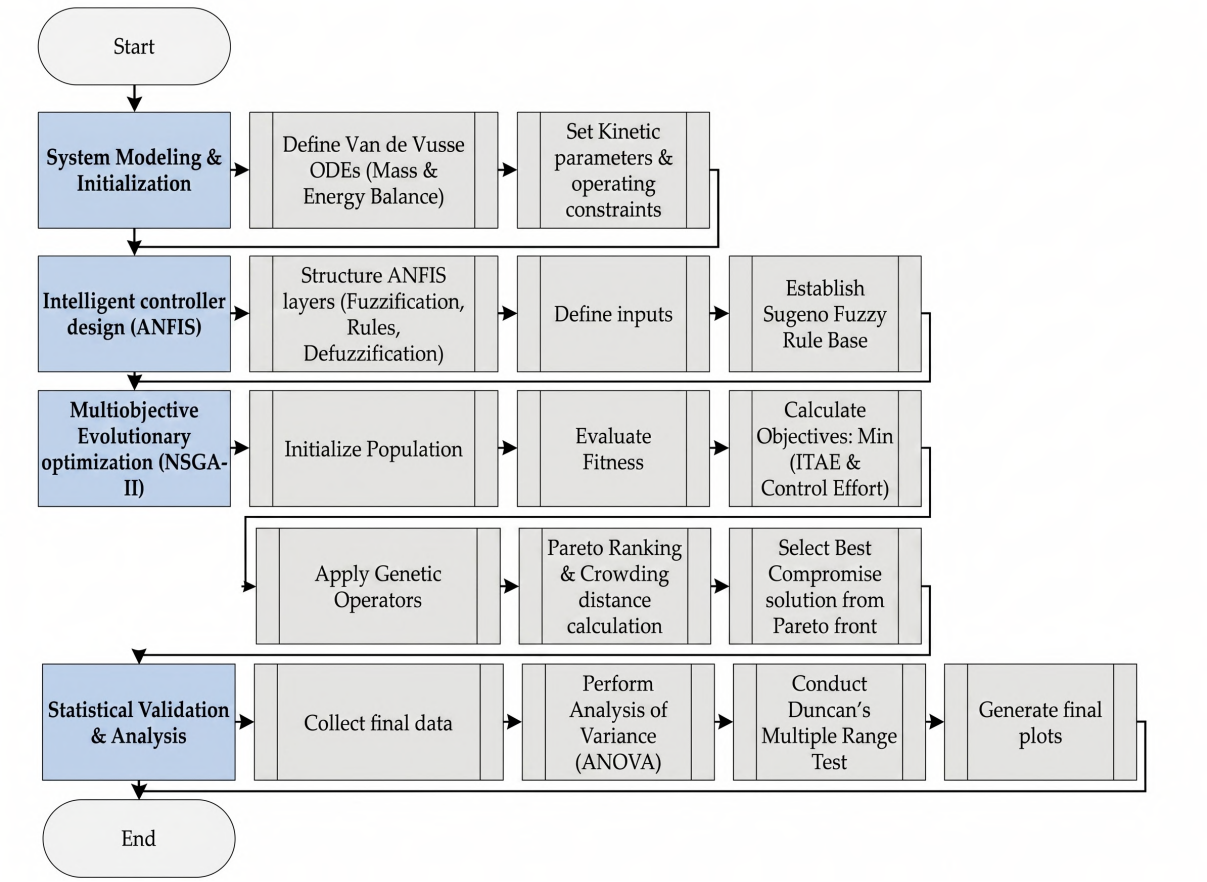

Figure 1 Research methodology adopted for the design, optimization, and validation of the neuro-fuzzy controller applied to the Van de Vusse reactor

2.1 Mathematical Modeling of the Van de Vusse Reactor

The proposed control strategy is validated using a continuous stirred tank reactor (CSTR) operating under the Van de Vusse reaction mechanism. This benchmark system involves a set of parallel and consecutive reactions (A → B → C and 2A → D), where the desired product is intermediate species B. This process exhibits highly nonlinear dynamics, multiple steady states, and non-minimum phase behavior (inverse response), particularly when the concentration of component B is controlled through the dilution rate.

To derive the dynamic mass and energy balances, the following mathematical model is developed:

- Perfect mixing: The concentration and temperature are uniformly distributed throughout the reactor.
- Constant volume and flow equilibrium: The reactor volume Vremains constant, and the inlet and outlet flow rates are equal (F_{in}=F_{out}=F), neglecting level dynamics.
- Constant physical properties: The fluid density ρ and heat capacity C_{p} are assumed constant.
- Heat transfer: Heat exchange is represented as a lumped parameter through an equivalent heat duty Q.
- Reaction kinetics: The kinetic rate constants depend on temperature following the Arrhenius law.

Dynamic model equations

- The mass balance for component A:

$$\frac{dC_A}{dt} = \frac{F}{V}(C_{A0} - C_A) - k_1(T)C_A - k_3(T)C_A^2 \tag{1}$$

- The mass balance for component B:

$$\frac{dC_B}{dt} = -\frac{F}{V}C_B + k_1(T)C_A - k_2(T)C_B \tag{2}$$

Energy balance:

$$\frac{dT}{dt} = \frac{F}{V}(T_0 - T) + \frac{1}{\rho C_p}\left[(-\Delta H_1)k_1(T)C_A + (-\Delta H_2)k_2(T)C_B + (-\Delta H_3)k_3(T)C_A^2\right] + \frac{Q}{\rho C_p V} \tag{3}$$

where C_A and C_B are the concentrations of species A and B (mol/L), Tis the reactor temperature (K), Fis the inlet flow rate (L/h), and Qis the heat removal rate (kJ/h). C_{A0}denotes the inlet concentration of species A, and T_0 is the inlet temperature. ΔH_i represents the heat of reaction, defined as negative for exothermic reactions.

- Kinetic expressions (Arrhenius law)

$$k_i(T) = k_{i0}\exp\left(\frac{-E_i}{RT}\right), \quad i = 1, 2, 3 \tag{4}$$

These assumptions are standard in the Van de Vusse reactor literature and allow nonlinear behavior analysis without introducing additional hydraulic complexity. Regarding the model parameters, the following values are used for simulation and are shown in Table 1.

The kinetic and thermodynamic parameters used in this study (Table 1) correspond to configurations commonly adopted in the literature for the Van de Vusse reactor as a benchmark system for nonlinear control. These values enable the reproduction of strongly nonlinear and coupled dynamics under realistic operating conditions.

The Arrhenius-based kinetic parameters introduce a pronounced temperature dependence, generating exponential nonlinearities that intensify the coupling between mass and energy balances. In addition, the presence of the parallel second-order reaction contributes to increased dynamic complexity and promotes non-minimum phase behavior, including inverse response in the concentration of the intermediate product.

The nominal operating conditions defined in Table 1 place the reactor near a highly sensitive region, allowing a proper evaluation of the controller's adaptive capability under strong thermokinetic interaction. The selected setpoint represents a physically attainable but demanding operating condition, ensuring a nontrivial control problem with a clear trade-off between tracking performance and energy usage.

Table 1 Kinetic and physical parameters of the reactor.

Parameter	Value	Units	Description
k_{10}	1.287×10^{12}	h^{-1}	Pre-exponential factor for the reaction $A \rightarrow B$
k_{20}	1.287×10^{12}	h^{-1}	Pre-exponential factor for the reaction $B \rightarrow C$
k_{30}	9.043×10^{9}	$L \cdot mol^{-1} \cdot h^{-1}$	Pre-exponential factor for the reaction $2A \rightarrow D$
E_1	9758.3	K	The activation energy of reaction 1
E_2	9758.3	K	The activation energy of reaction 2
E_3	8560.0	K	The activation energy of reaction 3
ΔH_1	-4.2	kJ/mol	Heat of the reaction $A \rightarrow B$
ΔH_2	-11.0	kJ/mol	Heat of the reaction $B \rightarrow C$
ΔH_3	-41.85	kJ/mol	Heat of the reaction $2A \rightarrow D$
ρ	0.9342	kg/L	Density
C_p	3.01	kJ/(kg·K)	Specific heat
V	10.0	L	Reactor volume
C_{A0}	5.1	mol/L	Inlet concentration
T_0	378.05	K	Inlet temperature (K)
F_{nom}	14.19	L/h	Nominal flow
Q_{nom}	-1113.5	kJ/h	Nominal heat duty
T_{safe}	420	K	The thermal safety limit

The thermal safety limit (Table 1) is incorporated as a constraint in the optimization process, preventing runaway conditions and restricting the search space to feasible regions. This constraint promotes solutions that balance tracking accuracy and actuator effort.

Finally, the use of constant physical properties and the selected reactor volume (Table 1) ensures appropriate numerical scaling for the integration of the dynamic model, maintaining computational stability during the repeated simulations required by the evolutionary algorithm.. The schematic model of the reactor is shown in Figure 2 below.

where:

F : Volumetric feed rate to the reactor

C_{A0} : Concentration of species A in the inlet stream

T_0 : Temperature of the inlet stream

C_B : Concentration of the intermediate product B

T : Reactor temperature

Chemical reactions:

$$A \xrightarrow{k_1} B, \quad B \xrightarrow{k_2} C, \quad 2A \xrightarrow{k_3} D$$

where k_1, k_2, k_3 are temperature-dependent kinetic constants (Arrhenius).
Q (Heat Duty): Heat flow supplied to or removed from the cooling/heating jacket
FCV : Flow control valve
TCV: Valve associated with the thermal system
FT: Flow transmitter
TT: Reactor temperature transmitter
AT (CB): Analyzer for concentration of species B
M: Agitator motor
CB: Concentration of the intermediate product B

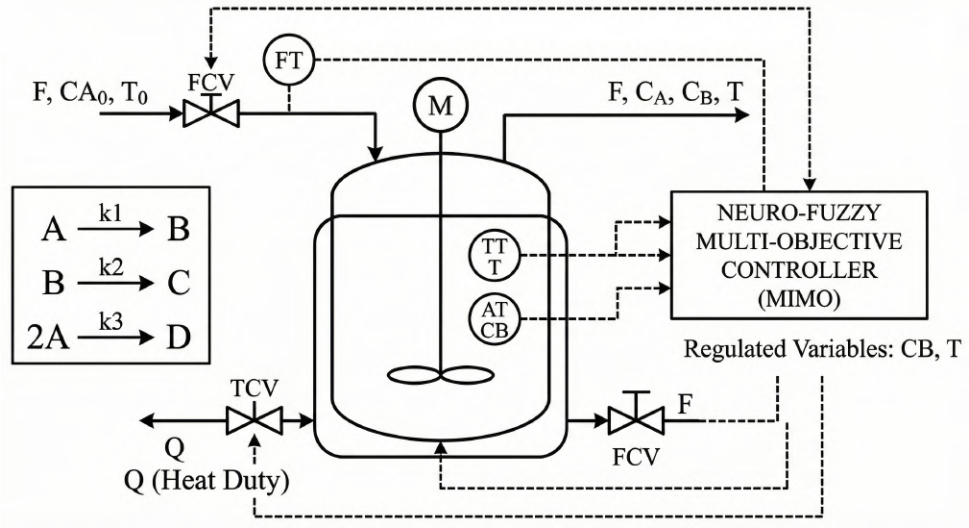

Figure 2 Schematic of the reactor

2.2 Design of the Neuro-Fuzzy Controller (ANFIS)

With the dynamic model defined, the design of the intelligent controller based on an Adaptive Neuro-Fuzzy Inference System (ANFIS) is carried out. This hybrid controller combines the universal approximation capability of neural networks with the interpretability of Sugeno-type fuzzy logic, allowing the modeling of complex nonlinear relationships between state variables and control actions. The implemented controller is a multiple input–multiple output (MIMO) controller that generates two manipulated signals simultaneously:

$$u(t) = \begin{bmatrix} F(t) \\ Q(t) \end{bmatrix}$$

where $F(t)$ is the feed flow and $Q(t)$ is the supplied or removed heat. This ANFIS uses the following as input variables:

- The concentration error is described in Equation (5):

$$e(t) = C_B^{ref} - C_B(t) \tag{5}$$

- The error derivative described in Equation (6):

$$\dot{e}(t) = \frac{e(t) - e(t - \Delta t)}{\Delta t} \tag{6}$$

- The integral of the error (parallel action) described in Equation (7):

$$e_i(t) = \int e(t)\, dt \tag{7}$$

While the fuzzy block employs e(t)and e (t), the integral action is incorporated in parallel with gains optimized by the evolutionary algorithm, allowing the elimination of steady-state error without excessively affecting transient stability. The implemented ANFIS structure comprises four functional layers:

Layer 1: Fuzzification

The model represents each input by Gaussian membership functions given by the following.:

$$\mu(x) = \exp\left(-\frac{(x-c)^2}{2\sigma^2}\right) \tag{8}$$

where cand σ are adjustable parameters encoded in the evolutionary chromosome. Three membership functions per variable are used to generate a smooth and differentiable fuzzy partition.

Layer 2: Inference

The fuzzy rules follow a first-order Sugeno structure, and each rule's activation is calculated using the product T-norm:

The fuzzy rules follow a first-order Sugeno structure, and each rule's activation is calculated using the product T-norm:

$$w_i = \mu_{e,i} \cdot \mu_{\dot{e},k} \tag{9}$$

Layer 3: Normalization

$$\hat{w}_i = \frac{w_i}{\sum_j w_j} \tag{10}$$

Layer 4: Defuzzification

The model obtains the fuzzy output for each actuator by a weighted average:

$$u_{\text{fuzzy}} = \frac{\sum_i w_i z_i}{\sum_i w_i} \tag{11}$$

where z_i represents the consequent weight associated with each rule (evolutionary parameters). To improve steady-state accuracy, a high-gain integral term is added as follows:

$$F(t) = F_{\text{nom}} + u_F^{\text{fuzzy}} + K_F^I e_I(t) \tag{12}$$

$$Q(t) = Q_{\text{nom}} + u_Q^{\text{fuzzy}} + K_Q^I e_I(t) \tag{13}$$

The gains K_I^F and K_I^Q are optimized within the evolutionary process. Anti-windup is implemented via integral term saturation. Likewise, to ensure physical feasibility, the manipulated signals are strictly bounded, making the problem more realistic by introducing an additional nonlinearity:

$$5 \leq F(t) \leq 120$$

$$-4000 \leq Q(t) \leq 4000$$

2.3 Evolutionary Parameterization of the Neuro-Fuzzy Controller

The proposed ANFIS structure is not trained using traditional gradient methods; instead, all adjustable parameters are directly optimized using the NSGA-II evolutionary algorithm. Each individual in the population represents a complete controller configuration encoded as a real-valued chromosome of length L_{chrom}=32.

The chromosomal vector is defined as follows:

$$\theta = [\theta_1, \theta_2, \ldots, \theta_{32}] \in [-2, 2]^{32}$$

The internal distribution of genes is organized into the following four functional blocks:

- Parameters of membership functions (Genes 1–12)

The first 12 genes determine the parameters of the Gaussian membership functions defined by Equation 8. Three centers and three widths are considered for each input variable, resulting in six parameters per variable. Consequently, with two input variables, the total number of parameters associated with the membership functions is twelve. During implementation, the widths are restricted to be positive to guarantee the mathematical and physical validity of the functions, applying a positivity-enforcement mechanism. In the implementation, the widths are forced to be positive by the following:

$$\sigma = \|\theta_i\| + \varepsilon \tag{14}$$

This avoids numerical degeneration and ensures well-defined functions. In general, these parameters determine the fuzzy partition of the error (ϵ) space, directly modifying the controller sensitivity in different operating regions.

- Rule Weights for the Flow Actuator F(Genes 13–21)

The next 9 positions of the chromosome correspond to the Sugeno-type rule consequents for the flow actuator. Because there are 3 membership functions for eand 3 for $\dot{e}$ a total of 3×3=9 fuzzy rules are generated.Each rule has a weight z_i^F that defines its contribution to the fuzzy output as follows:

$$F_{\text{fuzzy}} = \frac{\sum_i w_i \, z_i^F}{\sum_i w_i} \tag{15}$$

where z_i^F is evolutionarily encoded. These genes determine the geometry of the control surface associated with the flow.

- Rule Weights for the Thermal Actuator Q(Genes 22–30)

Analogously, the next 9 genes define the consequents of the same 9 rules, but associated with the thermal actuator:

$$Q_{\text{fuzzy}} = \frac{\sum_i w_i \, z_i^Q}{\sum_i w_i} \tag{16}$$

This allows both outputs to share the same inference structure while having independent control surfaces, which is an essential characteristic of a MIMO controller.

- Integral Gains (Genes 31–32)

The last two genes correspond to the integral gains K_i^F and K_i^Q. These gains scale the integral terms in Eqs. (12) and (13).

The evolutionary inclusion of these parameters enables the automatic tuning of steady-state error elimination, convergence speed, and control aggressiveness.

2.4 Formulation of the Multi-Objective Optimization Problem

Let the nonlinear model of the VDR be defined as

$$\dot{x}(t) = f(x(t), u(t)), \quad x(0) = x_0 \tag{17}$$

with

$$x(t) = \begin{bmatrix} C_A(t) \\ C_B(t) \\ T(t) \end{bmatrix}$$

and an integral NFC:

$$u(t) = G(e(t), \dot{e}(t), e_I(t); \theta)$$

where $\theta \in [-2, 2]^{32}$ is the optimized parameter vector.

The control objective is to regulate the following:

$$C_B(t) \to C_B^{ref} = 1.12 \text{ mol/L}$$

System performance is evaluated using two complementary criteria:

- ITAE (Integral of Time-Weighted Absolute Error)

  This index penalizes persistent errors over time, promotes fast responses, and reduces long settling tails (Eq. 9):

$$f_1(\theta) = \int_0^{T_{\text{sim}}} t \, |e(t; \theta)| \, dt \tag{18}$$

Control Effort
The effort is quantified using the quadratic variation of the manipulated signals (Eq. 10):

$$f_2(\theta) = \int_0^{T_{\text{sim}}} \|\Delta u(t; \theta)\|^2 \, dt \tag{19}$$

where:

$$\Delta u(t) = u(t) - u(t - \Delta t) \tag{20}$$

This term penalizes aggressive actions, reduces physical wear, and limits energy consumption.

Under the above considerations, the multi-objective problem can be defined as follows:

$$\min_{\theta \in \Omega} F(\theta) = \begin{bmatrix} f_1(\theta) \\ f_2(\theta) \end{bmatrix}$$

subject to

$$\dot{x} = f(x, G(x; \theta)), \quad T(t) \leq T_{\text{safe}}, \quad u(t) \in U, \quad \Omega = [-2, 2]^{32}$$

The objective functions exhibit an inherent conflict between achieving fast responses and maintaining smoothness and low energy usage (effort). In general, this trade-off can be summarized as follows: “greater speed implies greater effort,” whereas “lower effort implies larger transient error.” Therefore, there is no single globally optimal solution, but rather a set of non-dominated solutions forming the Pareto front. To solve the problem, the following algorithm was implemented in pseudocode using the Python programming language, together with the previously described model.

Algorithm 1 NSGA-II-based ANFIS controller optimization

Input: $N_{pop} = 100$, $G_{max} = 40$, $L_{chrom} = 32$, $\Delta t = 0.05$, $N_{train} = 200$, $N_{val} = 600$, $C_B^{ref} = 1.12$, $T_{safe} = 420$ K, $F_{nom} = 14.19$, $Q_{nom} = -1113.5$, $F \in [5, 120]$, $Q \in [-4000, 4000]$

Output: Pareto front FP^*, best solution θ_{best}

Initialization

Define objective functions: $f_1 = \text{ITAE} = \int t|e(t)|dt$

Define control effort: $f_2 = \text{Control Effort} = \int \|\Delta u(t)\|^2 dt$

Initialize population $P_0 \in \mathbb{R}^{32}$ uniformly in $[-2, 2]$

Chromosome structure: 12 MF parameters, 9 rule consequents for F, 9 rule consequents for Q, and 2 integral gains (K_i^F, K_i^Q)

Evolutionary Loop (NSGA-II)

For $g = 1$ to $G_{max} = 40$

For each individual $\theta \in P_g$

Initialize state: $x_0 = [C_A, C_B, T] = [2.14, 1.09, 387.34]$

Initialize control: $u_0 = [F_{nom}, Q_{nom}]$, $e_0 = 0$, and $\int e = 0$

For $k = 1$ to $N_{train} = 200$

Measure output with noise: $C_B^{meas} = C_B + \mathcal{N}(0, 0.01)$

Compute error: $e = C_B^{ref} - C_B^{meas}$

Compute error derivative: $\dot{e} = \dfrac{e - e_{prev}}{\Delta t}$

Update integral term with saturation: $\int e = \text{clip}(\int e + e\Delta t, -50, 50)$

Compute ANFIS control using 3 Gaussian MFs per input, 9 rules, and weighted average inference

Control law for flow rate: $F = F_{nom} + \Delta F_{fuzzy} + K_i^F \int e$

Control law for heat duty: $Q = Q_{nom} + \Delta Q_{fuzzy} + K_i^Q \int e$

Apply saturation: $F \in [5, 120]$ and $Q \in [-4000, 4000]$

Integrate reactor model using ODEINT: $x_{k+1} = \text{ODE}(x_k, u_k, \Delta t)$

Accumulate ITAE objective: $f_1 += t|e|\Delta t$

Accumulate control effort: $f_2 += \|u_k - u_{k-1}\|^2 \Delta t$

If $T > 420$ or $T < 200$, apply penalty: $f_1 = f_2 = 10^9$

Selection and Variation

Merge parent and offspring populations

Perform non-dominated sorting

Compute crowding distance

Select top N_{pop} individuals

Apply binary tournament selection

Apply SBX crossover with probability 0.7 and distribution index $\eta = 20$

Apply polynomial mutation with probability 0.3, gene mutation probability 0.1, and distribution index $\eta = 20$

Generate offspring Q_g

Post-Processing and Validation

Extract Pareto front FP^*

Normalize objectives: $f_i^{norm} = \dfrac{f_i - f_i^{min}}{f_i^{max} - f_i^{min}}$

Select compromise solution: $\theta_{best} = \arg\min_{\theta \in FP^*} \sqrt{(f_1^{norm})^2 + (f_2^{norm})^2}$

Simulate best controller for $N_{val} = 600$ steps
Perform robustness test by perturbing k_1 by $\pm 10\%$
Report tracking performance, temperature evolution, and control signals
Return: Pareto front FP^*, best solution θ_{best}, and performance metrics

3. Results and Discussion

3.1 Algorithm stability and Pareto front analysis

To address the stochastic nature of evolutionary algorithms and ensure the optimization's reproducibility, the NSGA-II algorithm was executed in five independent runs using different random initialization seeds. The algorithm consistently converged to a well-defined convex Pareto front across all executions (Figure 3), confirming the conflicting nature between control accuracy (ITAE) and energy efficiency (control effort) (Rangaiah et al., 2020; Verma et al., 2021).

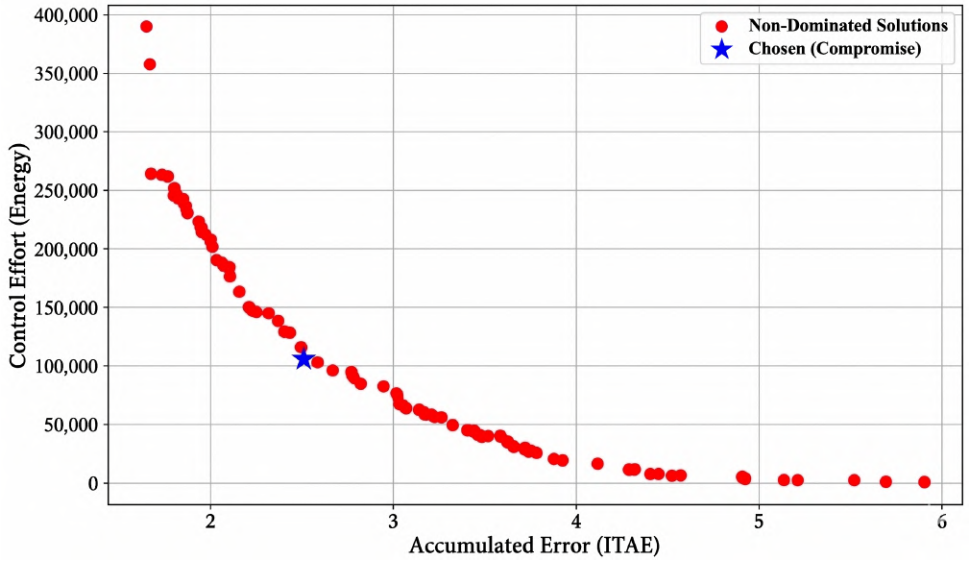

Figure 3 Pareto front illustrating the trade-off between tracking error (ITAE) and control effort. Red markers denote non-dominated solutions, whereas the blue star represents the chosen compromise solution

Analysis of the Pareto boundary shows that reducing the ITAE below 2.0 entails an increasing marginal energy cost, diminishing returns in control aggressiveness. The selected compromise solution (ITAE = 2.51, Effort = 1.05×10^5) is strategically located in the knee region of the curve. This validates the proposed method's ability to identify configurations that ensure high dynamic performance while avoiding premature actuator wear.

3.2 Comparative performance analysis: ANFIS vs. classical baseline

To benchmark the efficacy of the proposed multi-objective ANFIS, its closed-loop performance was directly compared with that of a classically tuned parallel Proportional-Integral-Derivative (PID) controller. The time-domain simulation results conclusively validate the proposed control scheme's superiority.

A comparative analysis was conducted to evaluate the effectiveness of the proposed NSGA-II optimized ANFIS controller against both a classical PID controller and a non-optimized ANFIS baseline. The results demonstrate a substantial improvement in control performance. The optimized ANFIS achieved an ITAE value of 2.51, compared to 159.17 obtained with the classical PID controller, representing a reduction of approximately 98.4% in accumulated tracking error. This result highlights the severe limitations of conventional linear control strategies when applied

to systems with strong nonlinearities and non-minimum phase behavior, such as the Van de Vusse reactor.

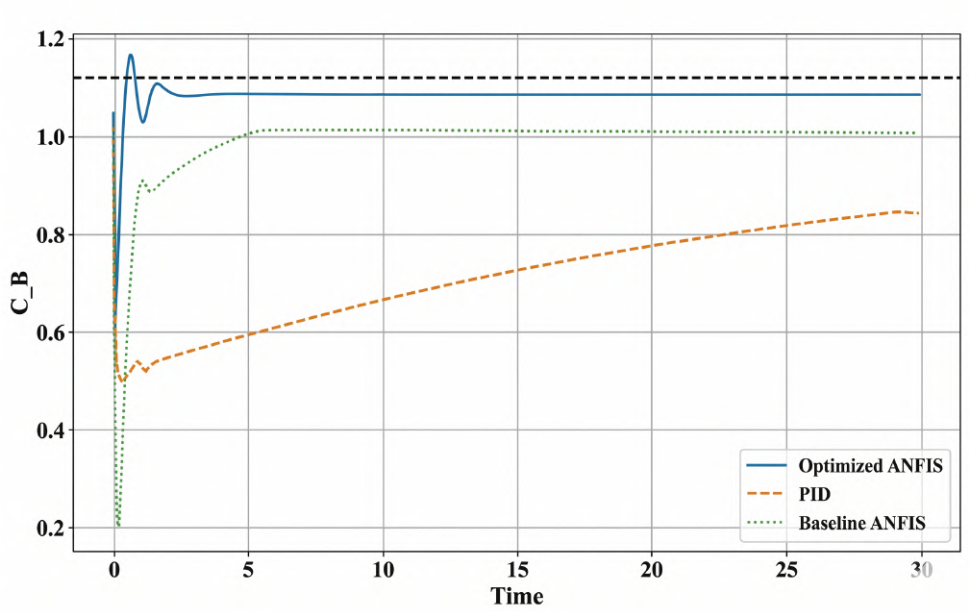

Figure 4 Performance Comparison: Optimized ANFIS vs. classical PID vs. baseline ANFIS

Furthermore, the comparison with a baseline ANFIS controller (ITAE = 50.29) confirms that the observed performance gain is primarily driven by the multi-objective evolutionary optimization process and not the neuro-fuzzy structure itself (Mohamed et al., 2025; Sevindik et al., 2024). The NSGA-II algorithm reduces ITAE by approximately 95.0% relative to the non-optimized ANFIS, demonstrating its effectiveness in tuning both the structural and parametric components of the controller.

The optimized ANFIS exhibits a significantly faster transient response and achieves the desired setpoint with negligible steady-state error from a dynamic perspective. In contrast, the classical PID controller shows a slow response and fails to reach the reference within the simulation horizon, whereas the baseline ANFIS provides moderate performance but remains suboptimal. These results confirm that the proposed ANFIS–NSGA-II framework effectively captures the system's nonlinear dynamics and provides a robust, high-performance, and scalable control solution for complex chemical processes.

In contrast, the optimized ANFIS controller successfully dominates the complex inverse dynamics (Alfaro-Balaguer et al., 2025; Williams, 2021). The ANFIS provides a highly decisive response by leveraging the nonlinear surface of its fuzzy rule base (Figure 5), overcoming the initial drop and settling near the target concentration (CB = 1.12 mol/L) in approximately 3 h.

Quantitatively, the proposed neuro-fuzzy approach achieved an outstanding ITAE of 2.51, representing an error reduction of over 98.4% compared with the classical baseline. Furthermore, the thermal response (Figure 5) demonstrates that the ANFIS inherently operates at a cooler, safer steady-state temperature (~385 K) than the PID, remaining strictly below the 420 K safety limit.

3.3 Actuator Constraints and Analysis of Saturation

From a practical process control perspective, continuous actuator saturation is typically treated as a warning sign. However, the control action profiles (Figure 4, bottom panel) reveal a critical physical insight regarding the Van de Vusse benchmark: the chosen nominal operating point (CB = 1.12 mol/L) lies at the reactor's productive capacity's extreme upper boundary.

Continuous maximum feed flow (F = 120 L/h) is mandatory to physically sustain this demanding concentration. The optimized ANFIS controller successfully identifies this requirement,

exhibiting an optimal time-response strategy (similar to a "bang-bang" control principle). It aggressively drives the actuator to its upper limit early in the transient phase to rapidly suppress the massive inverse error and maintains it to lock in the setpoint. Conversely, the classical PID is too conservative and sluggish, slowly ramping up the flow and consequently starving the reactor of the necessary reactant to reach the setpoint in a timely manner. This demonstrates that the saturation observed in the neuro-fuzzy controller is not an algorithm flaw, but rather an optimal and necessary physical action to meet the plant's stringent productivity demands without violating thermal safety constraints.

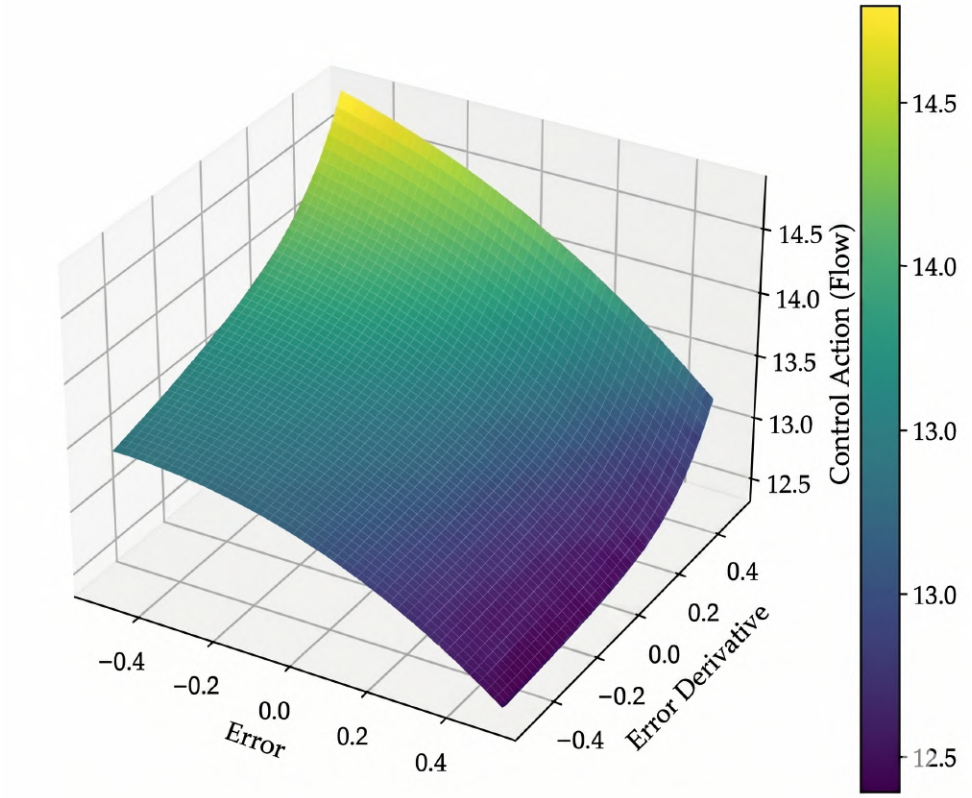

Figure 5 Three-dimensional control surface generated by the optimized ANFIS controller, illustrating the relationship between the tracking error, error derivative, and flow control action

3.4 Robustness under Parametric Uncertainty

A robustness test was performed to evaluate the controller under parametric uncertainties of ±10% in the reaction kinetics (Figure 6).

The robustness analysis reveals that the controller guarantees the system's asymptotic stability. The accelerated-kinetics scenario (+10%) maintains accurate tracking. The reduced-kinetics scenario (-10%) exhibits a slight irreducible steady-state error (CB ≈ 1.02 mol/L), confirming that the nominal operating point lies at the absolute boundary of the reactor's productive capacity under those specific kinetic conditions. The controller behaves robustly and is limited only by plant physics rather than by the control logic.

3.5 Validation

A targeted two-factor ANOVA (with interaction) was conducted to evaluate the sensitivity of system performance (ITAE) to variations in the integral gains $K_(i, F)$and $K_(i, Q)$. Each factor was analyzed at three levels with four replicates per treatment, using ITAE as the performance metric. Independent replicates correspond to distinct dynamic conditions (or randomly seeded noise realizations).

A two-factor factorial analysis of variance (ANOVA) was performed to evaluate the influence of the integral gains associated with the flow (F) and thermal (Q) loops on system performance. Each factor was studied at three levels (low, medium, and high), forming a fully crossed 3×3 design with four replicates per treatment. The ITAE index was selected for its ability to penalize persistent errors and reflect overall temporal response quality.

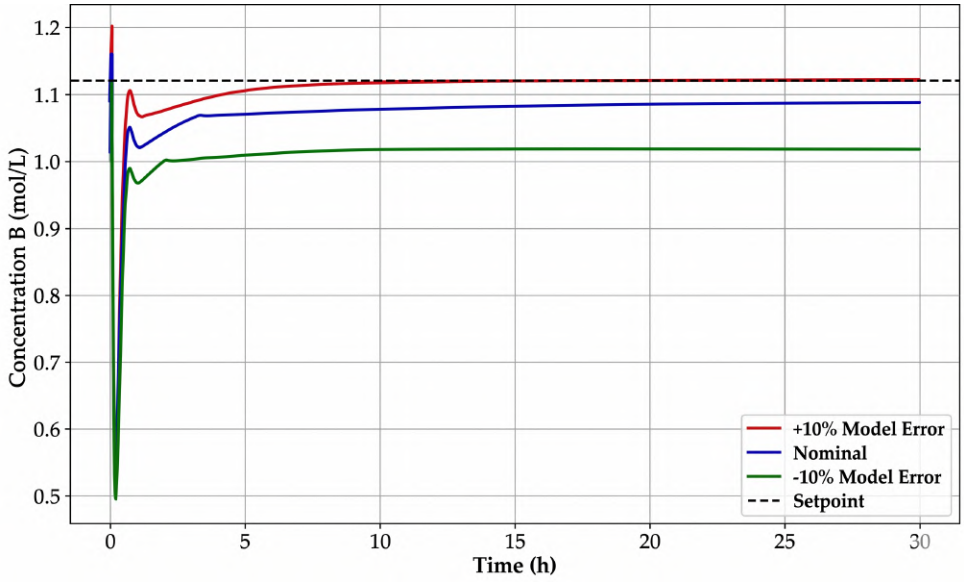

Figure 6 Robustness test: variation in reaction kinetics

The statistical model used is expressed as (Equation 21):

$$Y_{ijk} = \mu + \alpha_i + \beta_j + (\alpha\beta)_{ij} + \varepsilon_{ijk} \tag{21}$$

where Y_{ijk} represents the observed ITAE value, μ is the overall mean, α_i and β_j correspond to the effects of factors K_i^F and K_i^Q, respectively, $(\alpha\beta)_{ij}$ is the interaction effect, and ε_{ijk} is the random error assumed to be independently and normally distributed with zero mean and constant variance. Table 2 shows the overall model metrics.

Table 2 General ANOVA model metrics

Variable	N	R^2	Adj. R^2	CV
ITAE	36	0.94	0.93	7.4

The coefficient of determination (R^2) is 0.94, meaning that 94% of the observed variability in ITAE is explained by the experimental design factors (Integral Gain of Flow and Heat). The coefficient of variation (CV) of 7.4% suggests acceptable experimental precision. Table 4 shows the statistical significance indicators of the model.

Table 3 ANOVA model

Source	SS	df	MS	F	P-value	Sig.
Model	1301.67	7	185.95	67.53	< 0.0001	***
K_i^F Level	1285.17	2	642.58	233.35	< 0.0001	***
K_i^Q Level	16.45	2	8.23	2.99	0.0667	*
$K_i^F \times K_i^Q$	76.19	4	19.05	531.50	< 0.0001	***
Error	77.11	27	2.75	—	—	—
Total	1378.77	35	—	—	—	—

The ANOVA results indicate that the integral gain associated with the flow loop ($K_{i,F}$) has a statistically significant effect on system performance ($p < 0.0001$), whereas the thermal

gain ($K_{i,Q}$) shows a weaker main effect. However, the interaction between both factors is highly significant ($p < 0.0001$), demonstrating that the influence of $K_{i,Q}$ depends on the level of $K_{i,F}$. This result highlights the coupled nature of the control inputs and confirms that coordinated tuning of both gains is required for optimal performance.

Given the strong effect of $K_{i,F}$, a Duncan post hoc test was conducted to analyze the differences between factor levels (Table 4). The results show that higher values of $K_{i,F}$ are associated with lower ITAE values, with statistically distinct groupings across low, medium, and high levels.

Table 4 Duncan Post hoc Test ($\alpha = 0.05$)

Level	Mean ITAE	n	Std. Error	Group
High	16.38	12	0.48	A
Medium	20.31	12	0.48	B
Low	30.55	12	0.48	C

Means sharing a common letter are not significantly different ($p > 0.05$).

While the ANOVA and Duncan tests provide useful insights into the influence of the integral gains and their interaction, it is important to contextualize these findings. Since this analysis focuses exclusively on two parameters while keeping the remaining controller parameters fixed, it represents a localized sensitivity analysis. Therefore, these results should be interpreted as supporting evidence for understanding the role of integral action, rather than as a comprehensive statistical validation of the entire multi-objective optimized controller.

3.6 Discussion

The Van de Vusse reactor is a challenging benchmark for advanced control because of its nonlinear dynamics, competitive and consecutive reactions, and non-minimum phase behavior (Hofer et al., 2023). The results show that the classical PID controller is unable to achieve the desired setpoint within the evaluated horizon, while the optimized neuro-fuzzy controller significantly improves tracking performance under the same simulation conditions. The improvement is mainly associated with the multi-objective NSGA-II optimization, since the non-optimized ANFIS baseline performs noticeably worse. The optimized controller also uses an aggressive initial feed-flow action that drives the actuator to saturation, which is consistent with the system's inverse-response dynamics and the selected operating point ($C_B \approx 1.12$ mol/L). In this context, the observed saturation reflects a physically meaningful control action rather than a design flaw.

The robustness test under ±10% kinetic perturbations confirms stable behavior within the evaluated scenario, although the analysis remains limited to parametric uncertainty (Williams, 2021; Govindharaj et al., 2024). Similarly, the ANOVA results should be interpreted as a localized sensitivity analysis because only the integral gains were varied while the remaining controller parameters were fixed. Overall, NSGA-II enabled a practical trade-off between tracking accuracy and control effort, but the conclusions should still be considered simulation-based proof of concept rather than full industrial validation.

4. Conclusions

This study presented a multi-objective neuro-fuzzy control framework integrating ANFIS and the NSGA-II evolutionary algorithm for stabilizing a Van de Vusse continuous stirred tank reactor, addressing the challenges posed by nonlinear dynamics and non-minimum phase behavior. The results obtained under simulation conditions show a significant improvement in control performance, with the optimized ANFIS achieving an ITAE of 2.51, corresponding to reductions of approximately 98.4% and 95.0% relative to a classical PID controller and a non-optimized ANFIS baseline, respectively, indicating the effectiveness of the multi-objective optimization in tuning both structural and parametric components. The controller demonstrates the ability to

compensate for inverse response dynamics and maintain operation within the thermal safety limits, where the observed actuator saturation is interpreted as a process-driven optimal response. Robustness analysis under ±10% parametric uncertainty confirms stable performance within the evaluated scenario; however, this assessment remains limited in scope because additional sources of uncertainty, such as measurement noise, actuator dynamics, and broader operating conditions, were not fully explored. Likewise, the statistical analysis based on a targeted ANOVA provides useful insight into the influence of integral gains but should be considered as supporting evidence rather than a comprehensive validation of the full controller structure. Overall, the proposed ANFIS–NSGA-II framework constitutes a simulation-based proof of concept that demonstrates its potential for nonlinear process control, although its general applicability to other industrial systems should be interpreted with caution. To assess practical feasibility, future work will focus on extending the validation through more comprehensive robustness analyses and experimental implementation, including hardware-in-the-loop and real-time testing.

Acknowledgements

The authors conducted this research independently and received no external support.

Author Contributions

Gustavo A. Flores Fernandez conceived the study, developed the methodology, modeled the neuro-fuzzy algorithm, implemented the algorithms, performed the simulations, and drafted the original manuscript. Miguel Jiménez-Carrión contributed to the conceptualization, neuro-fuzzy algorithm modeling, supervision, and critical revision of the manuscript. María L. Muro Zúñiga contributed to data analysis, reactor modeling, validation of results, and manuscript review. Juan M. Oliva Núñez assisted with the experimental design, methodological review, and technical editing. María Y. Albuquerque Trelles contributed to supervision, interpretation of results, and final approval of the manuscript. All authors reviewed and approved the final version of the manuscript.

Conflict of Interest

The authors declare no conflicts of interest.

References

Aghbashlo, M., Hosseinpour, S., & Tabatabaei, M. (2016). Exergetic optimization of continuous photobiological hydrogen production using hybrid anfis–nsga-ii. *Energy*, *96*, 507–520. https://doi.org/10.1016/j.energy.2015.12.084

Aguilar-López, R., Mata-Machuca, J., & Godinez-Cantillo, V. (2021). Tito control strategy for uncertain exothermic reactors. *Processes*, *9*(5), 873. https://doi.org/10.3390/pr9050873

Alfaro-Balaguer, V., Vega, S., Iza, J., Robalino, I., Rueda, M., Sinchiguano, P., & Camacho, O. (2025). Control of inverse response processes by direct synthesis control: A cstr case study. *IEEE Colombian Conference on Automatic Control (CCAC)*. https://doi.org/10.1109/CCAC64704.2025.11259301

Åström, K., & Hägglund, T. (2006). *Advanced pid control*. ISA.

Bagheri, P., & Khodabakhshian, A. (2014). Nsga-ii based multiobjective pid controller tuning for dc motor drives. *International Journal of Power Electronics and Drive Systems*, *4*(3), 322–330. https://doi.org/10.11591/ijpeds.v4i3.5976

Bagheri, P., & Mognjerdi, A. (2013). Multi-objective optimization of anfis structure. *International Conference on Intelligent and Advanced Systems*. https://doi.org/10.1109/ICIAS.2007.4658384

Bertone, A., Jafelice, R., & Goes, B. (2018). Classic and fuzzy type-2 control for the van de vusse reactor. *Trends in Computational and Applied Mathematics*, *19*(2), 258–270. https://doi.org/10.5540/03.2018.006.02.0258

Coello Coello, C. (2004). *Evolutionary multiobjective optimization: Theoretical advances and applications*. Springer. https://doi.org/10.1007/978-1-4757-5184-0

Coello Coello, C. (2006). Evolutionary multi-objective optimization: A historical view of the field. *IEEE Computational Intelligence Magazine*, *1*(1), 28–36. https://doi.org/10.1109/MCI.2006.1597059

Davila, J., Fridman, L., & Levant, A. (2005). Second-order sliding-mode observer for mechanical systems. *IEEE Transactions on Automatic Control*, *50*(11), 1785–1789. https://doi.org/10.1109/TAC.2005.858636

Deb, K., Pratap, A., Agarwal, S., & Meyarivan, T. (2002). A fast and elitist multiobjective genetic algorithm: Nsga-ii. *IEEE Transactions on Evolutionary Computation*, *6*(2), 182–197. https://doi.org/10.1109/4235.996017

Dostal, P., & Bobal, V. (2012). Neuro-fuzzy control design of chemical processes. *Foundations of Computing and Decision Sciences*, *37*(4), 255–266. https://doi.org/10.2478/v10209-011-0014-6

Fraga, E. (2019). Multi-objective optimization for dynamic processes. *Chemical Engineering Transactions*, *74*, 601–606. https://doi.org/10.3303/CET1974101

Govindharaj, I., Dinesh Kumar, K., Balamurugan, S., Yazhinian, S., Anandh, R., et al. (2024). Sensorless vector-controlled induction motor drives: Boosting performance with adaptive neuro-fuzzy inference system integrated augmented mras. *MethodsX*, *13*, 102992. https://doi.org/10.1016/j.mex.2024.102992

Hesami, M., Alizadeh, M., Naderi, R., & Tohidfar, M. (2020). Forecasting and optimizing agrobacterium-mediated genetic transformation via ensemble model–fruit fly optimization algorithm: A data mining approach using chrysanthemum databases. *PLoS ONE*, *15*(9), e0239901. https://doi.org/10.1371/journal.pone.0239901

Hofer, A., Matušů, R., Prokop, R., & Vojtěšek, J. (2023). Nonlinear control of van de vusse reactor using feedback linearization. *Chemical Engineering Science*, *265*, 118223. https://doi.org/10.1016/j.ces.2023.118223

Jiang, Q., & Wang, P. (2025). Nsga-ii algorithm based control parameters optimization strategy for megawatt novel nuclear power systems. *Energy*, *316*, 134444. https://doi.org/10.1016/j.energy.2025.134444

Lamba, R., & Raghu, N. (2013). Analysis of van de vusse reactor using model predictive control. *International Journal of Emerging Technology and Advanced Engineering*, *3*(6), 236–240.

Lima, F., Faria, R., Curvelo, R., Cadorini, M., Echeverry, C., de Souza, M. J., & Secchi, A. (2023). Nonlinear model predictive control approaches for a van de vusse reactor. *Processes*, *11*(4), 1102. https://doi.org/10.3390/pr11041102

Liu, C., Liu, C., & Li, J. (2025). Multi-model collaborative optimization using nsga-ii decision framework. *Metals*, *15*(8), 905. https://doi.org/10.3390/met15080905

Liu, Y., Chu, M., Ye, Q., Li, J., & Han, D. (2024). Multi-objective optimization of fcc separation system based on nsga-ii. *Chemical Engineering Science*, *302*, 120829. https://doi.org/10.1016/j.ces.2024.120829

Mohamed, Z., Ali, A., & Dabour, W. (2025). Optimizing adaptive neuro-fuzzy inference system model based chaotic harris hawks algorithm for stock prediction. *Scientific Reports*, *15*, 32529. https://doi.org/10.1038/s41598-025-15022-8

Mousavi, S., Castellanos-Cárdenas, D., Posada, N., Orozco-Duque, A., Sepúlveda-Cano, L., Castrillón, F., Camacho, O., & Vásquez, R. (2024). A review on data-driven model-free sliding mode control. *Algorithms*, *17*(12), 543. https://doi.org/10.3390/a17120543

Odwyer, A. (2009). *Handbook of pi and pid controller tuning rules* (3rd ed.). Imperial College Press. https://doi.org/10.1142/p575

Prokop, R., Matušů, R., & Vojtěšek, J. (2020). Feedback control of chemical reactors by modern principles. *Chemical Engineering Transactions*, *81*, 805–810. https://doi.org/10.3303/CET2081135

Rahman, A., Ihsan, S., & Hassan, N. (2022). A fuzzy-logic-controlled two-speed electromagnetic gearbox for electric vehicles. *International Journal of Technology*, *13*(2), 297–309. https://doi.org/10.14716/ijtech.v13i2.3913

Rangaiah, G., Feng, Z., & Hoadley, A. (2020). Multi-objective optimization applications in chemical process engineering: Tutorial and review. *Processes*, *8*(5), 508. https://doi.org/10.3390/pr8050508

Reyes, O., Sánchez, G., & Strefezza, M. (2009). Multi-objective genetic algorithm for tuning a neuro-fuzzy controller. *ICINCO*, *2*, 383–386. https://doi.org/10.5220/0002210103830386

Seborg, D., Edgar, T., Mellichamp, D., & Doyle, F. (2010). *Process dynamics and control* (3rd ed.). Wiley.

Sevindik, M., Gürgen, A., Krupodorova, T., Uysal, İ., & Koçer, O. (2024). A hybrid artificial neural network and multi-objective genetic algorithm approach to optimize extraction conditions of mentha longifolia and biological activities. *Scientific Reports*, *14*, 31403. https://doi.org/10.1038/s41598-024-83029-8

Talpur, N., Abdulkadir, S., Alhussian, H., Hasan, M., & Khan, M. (2023). Deep neuro-fuzzy system application trends, challenges, and future perspectives: A systematic survey. *Artificial Intelligence Review*, *56*(2), 865–913. https://doi.org/10.1007/s10462-022-10188-3

Velioglu, M., Zhai, S., Rupprecht, S., Mitsos, A., Jupke, A., & Dahmen, M. (2024). Physics-informed neural networks for dynamic process operations. *Computers & Chemical Engineering*, *192*, 108899. https://doi.org/10.1016/j.compchemeng.2024.108899

Verma, S., Pant, M., & Snášel, V. (2021). A comprehensive review on nsga-ii for multi-objective combinatorial optimization problems. *IEEE Access*, *9*, 175809–175828. https://doi.org/10.1109/ACCESS.2021.3070634

Widiatmoko, P., Devianto, H., Irawan, S., Vinka, A., Sukmana, I., Saputera, W., Eviani, M., & Prakoso, T. (2025). Optimizing reactor configuration and electrode geometry for enhanced electrochemical reduction of co_2. *International Journal of Technology*, *16*(6), 1956–1968. https://doi.org/10.14716/ijtech.v16i6.7547

Williams, A. (2021). Performance and robustness of alternate nonlinear control system designs for a nonlinear isothermal cstr. *IFAC-PapersOnLine*, *54*(21), 127–132. https://doi.org/10.1016/j.ifacol.2021.12.022

Zhu, B., Liu, L., Zhang, L., Liu, M., Duanmu, Y., Chen, Y., Dang, P., & Li, J. (2022). A variable-order fuzzy logic controller design method for an unmanned underwater vehicle based on nsga-ii. *Fractal and Fractional*, *6*(10), 577. https://doi.org/10.3390/fractalfract6100577